Journal of Nuclear Materials 404 (2010) 203–209

Contents lists available at ScienceDirect

Journal of Nuclear Materials

journal homepage: www.elsevier.com/locate/jnucmat

Mechanical properties of Y_2O_3-doped W–Ti alloys

M.V. Aguirre [a], A. Martín [b], J.Y. Pastor [b], J. LLorca [b,c,*], M.A. Monge [d], R. Pareja [d]

[a] Departamento de Tecnologías Especiales Aplicadas a la Aeronáutica, Universidad Politécnica de Madrid, Escuela de Ingeniería Aeronáutica y del Espacio, 28040 Madrid, Spain
[b] Departamento de Ciencia de Materiales-CISDEM, Universidad Politécnica de Madrid, E. T. S. de Ingenieros de Caminos, 28040 Madrid, Spain
[c] Instituto Madrileño de Estudios Avanzados de Materiales (Instituto IMDEA Materiales), C/ Profesor Aranguren s/n, 28040 Madrid, Spain
[d] Departamento de Física, Universidad Carlos III de Madrid, 28911 Leganés, Spain

ARTICLE INFO

Article history:
Received 13 May 2010
Accepted 8 July 2010

ABSTRACT

W and W alloys are currently considered promising candidates for plasma facing components in future fusion reactors but most of the information on their mechanical properties at elevated temperature was obtained in the 1960s and 1970s. In this investigation, the strength and toughness of novel Y_2O_3-doped W–Ti alloys manufactured by powder metallurgy were measured from 25 °C up to 1000 °C in laboratory air and the corresponding deformation and failure micromechanisms were ascertained from analyses of the fracture surfaces. Although the materials were fairly brittle at ambient temperature, the strength and toughness increased with temperature and Ti content up to 600 °C. Beyond this temperature, oxidation impaired the mechanical properties but the presence of Y_2O_3 enhanced the strength and toughness retention up to 800 °C.

1. Introduction

The design of future fusion reactors demands the availability of plasma facing components (PFCs) fabricated with materials that can withstand extreme conditions of temperature, irradiation and thermal stresses. These plasma facing materials (PFMs) have to present high melting temperature, good thermal conductivity, thermal shock resistance, minimal tritium retention, low sputtering and erosion rates and, furthermore, be resistant to damage induced by fusion neutrons. W has all these properties and is being considered as potential PFM.

Experiments carried out with W coated PFCs in ASDEX Upgrade have demonstrated the viability of W as a PFM and its advantages for high-heat flux components under plasma operation in steady state conditions [1–3], though the use of W in structural applications is limited because of its high ductile–brittle transition temperature (DBTT) and poor ductility. However, pure W and some oxide dispersed strengthened W alloys, such as W–1%La_2O_3 (WL10) or K-doped alloys (WVM), have been envisaged as potential structural materials in the modular He-cooled divertor concept of the near-term demonstration reactor DEMO [4]. The operating temperature window (OTW) for these materials appears to be presently established between 800 °C and 1200 °C according to the reported values for their DBTT and recrystallization temperature (RCT) [4–6]. The required OTW for the structural materials of the thimble and cooling unit of a modular He-cooled divertor should be between 600 °C and 1300 °C, at least [4]. Subsequently, a requirement of the divertor design is the development of W alloys having DBTT values somewhat below 600 °C and RCT around 1300 °C.

The first studies on the mechanical behavior of W and W alloys at high temperature were published around 1960. They were devoted to analyze the evolution of mechanical properties (mainly yield strength and ductility) with temperature and in the determination of the parameters that control the DBTT [7–11]. The recent interest in these materials for fusion reactors has led to the exploration of new ways to improve these properties. For instance, it has been shown that La_2O_3 dispersion or Al–K–Si doping can significantly improve the mechanical strength and the RCT of W, but it appears that the DBTT cannot be lowered this way [6,12–14]. Y_2O_3 additions strengthen W and increase its creep resistance [15,16] and it has recently been reported that Y_2O_3-doped W produced by powder metallurgy (PM) and consolidated by hot isostatic pressing (HIP) achieves certain ductility at 400 °C [17]. In addition, this Y_2O_3-doped W presented enhanced mechanical properties and a remarkable oxidation resistance at high temperatures, in comparison to W produced by the same procedure [17].

After rejecting the W–Re alloys for economic and practical reasons, it has been put forward that sintered W heavy alloys (WHA) might fulfill the requirements of the current divertor designs. In particular, W–(3–5)%Ni–(1–2)%Fe alloys have been proposed [6]. Nevertheless, other WHAs, for instance W–Ti and W–V, might exhibit more suitable characteristics for divertor applications because they would have less induced activation and, in all likelihood, a higher melting point and more favorable microstructure.

* Corresponding author at: Departamento de Ciencia de Materiales & CISDEM, Universidad Politécnica de Madrid. E. T. S. de Ingenieros de Caminos, 28040 Madrid, Spain.
E-mail address: jllorca@mater.upm.es (J. LLorca).

0022-3115/$ - see front matter © 2010 Elsevier B.V. All rights reserved.
doi:10.1016/j.jnucmat.2010.07.016

In particular, the bonding by means of a Ti-interlayer between the thermal armor of sintered W and a thimble made of W–Ti would be expected to be more effective than in the case of a WL10 thimble. The bonding between sintered W and WL10 appears to be successfully accomplished using a Ti-interlayer [18]. The mechanical behavior of W–4%Ti in the range 25–1000 °C has been reported elsewhere [17]. This alloy exhibited enhanced strength and brittle behavior up to 1000 °C. The extensive oxidation observed in the tested samples of this alloy was responsible for the degradation of the strength and toughness at high temperature. A Y_2O_3 dispersion, apart from strengthening the matrix and inhibiting grain growth, enhances oxidation resistance. In particular, it has been found that 0.5 wt.% Y_2O_3 addition remarkably enhances the oxidation resistance of PM W [17,19]. Accordingly, it should be expected that Y_2O_3 addition contributes to improving the mechanical behavior of W–Ti heavy alloys. Following these ideas, this work was aimed at investigating the mechanical behavior and fracture characteristics of PM W–2%Ti–0.5%Y_2O_3 and W–4%Ti–0.5%Y_2O_3 in the temperature range 25–1000 °C. It was decided to test in air to check the benefits provided by the inhibition of oxidation due to Y_2O_3 at very high temperature (>600 °C). Tests in vacuum are planned in the near future.

2. Materials and experimental methods

2.1. Materials

Two tungsten alloys with compositions W–2 wt.% Ti–0.50 wt.% Y_2O_3 and W–4 wt.% Ti–0.50 wt.% Y_2O_3 were studied. The starting powders were 99.9% pure W and 99.8% pure Ti with an average particle size of 14 and 20 μm, respectively, and nanometric particles of 99.5% pure monoclinic Y_2O_3 with sizes between 10 nm and 50 nm. The powder blends with the target compositions were milled inside a WC vessel sealed under a high purity Ar atmosphere, for 2 h in a high-energy planetary mill using WC balls of 10 mm in diameter as grinding media. The milled powders were introduced in stainless steel cans and degassed at 400 °C for 24 h and then the cans were vacuum sealed. The starting powders, as well as the blends and milled powders, were handled in each step of the procedure under a high purity Ar atmosphere using a glove box.

Cylindrical billets of 30 mm in diameter and 50 mm in length were obtained after consolidation by hot isostatic pressing at 195 MPa in two stages: the first one at 1277 °C for 2 h and the second one at 1700 °C for 30 min [4]. It should be noted that the

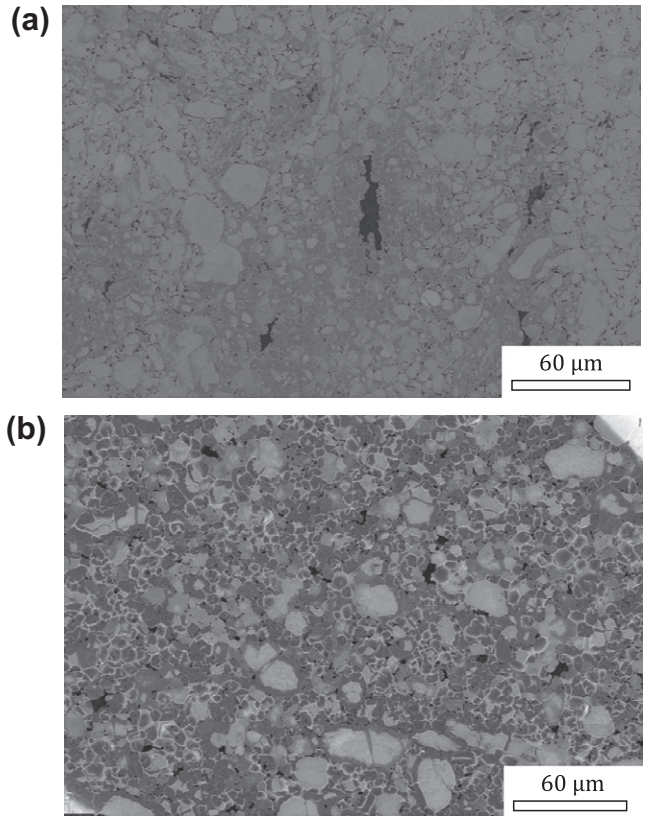

Fig. 1. Scanning electron micrographs of a polished section of (a) W–2Ti–0.5Y_2O_3 and (b) W–4Ti–0.5Y_2O_3 showing the details of the microstructure. W grains are light grey, α-Ti pools are black and Ti(W) solid solutions are dark grey.

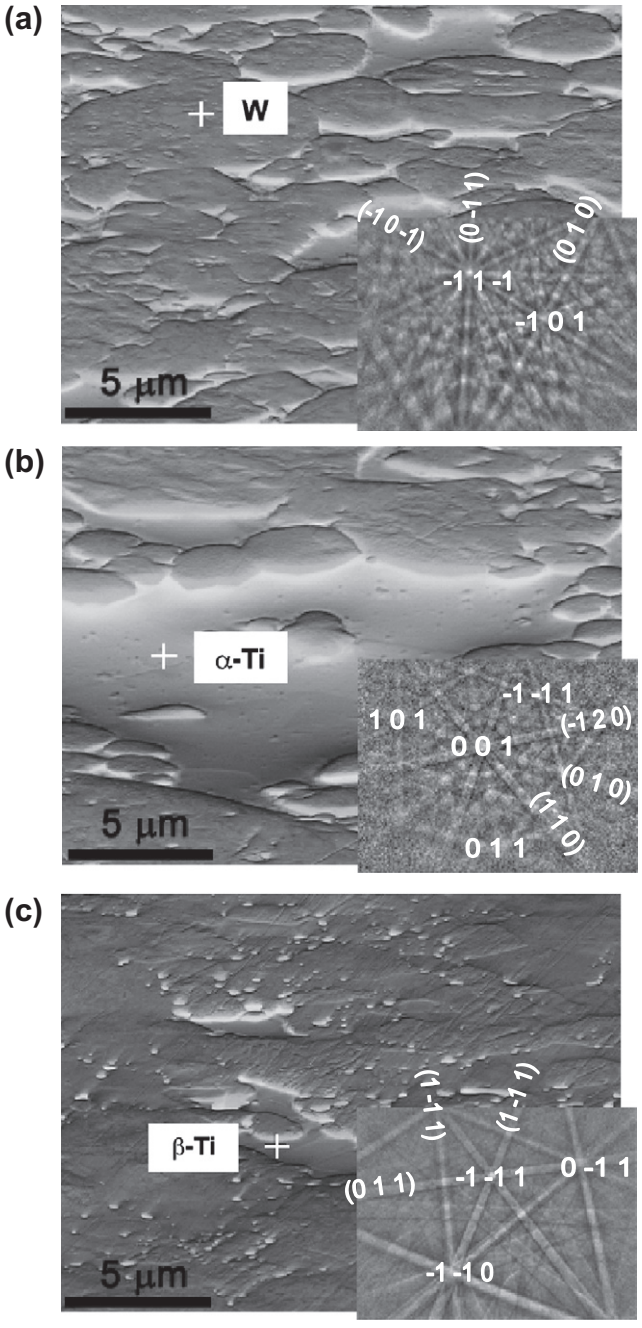

Fig. 2. Secondary electron images of W–4Ti–0.5Y_2O_3 and EBSD patterns from the regions indicated in the images. The EBSD patterns match the phases (a) W, (b) α-Ti and (c) β-Ti(W).

temperature of the second stage exceeded the melting point of Ti. Prismatic bars (nominal dimensions $2 \times 2 \times 25\ mm^3$) were prepared by refrigerated electro-discharge machining. They were annealed at 1000 °C for 1 h in a vacuum in order to remove residual stresses introduced during machining.

2.2. Experimental methods

The density of the samples was measured using Archimedes' immersion method with high purity ethanol. Vickers hardness was measured following the procedure indicated in ASTM standard 384-89 using loads of 9.8 and 98 N for 12 s.

Three-point bending tests were carried out on smooth and notched prismatic bars in a universal electromechanical testing machine. The bars were tested until fracture in a ceramic three-point bending fixture at different temperatures in the range 25–1000 °C in ambient atmosphere. The loading spans were 16 mm and 12 mm, respectively, for the tests on smooth and notched bars and the cross-section was always $2 \times 2\ mm^2$. Samples for fracture toughness tests were notched (not precracked) with a diamond saw. The notch depth was 400 μm and the notch tip radius was approximately 150 μm.

The bending fixture, connected to the actuator and the frame of the testing machine by ceramic bars, was placed in a high temperature furnace to carry out the tests. The specimens were heated at 50 °C/min and held at the test temperature for 15 min before testing. All mechanical tests were performed under stroke control at 100 μm/min. Load and displacement of the load point were continuously monitored during testing by means of a load cell and a linear variable differential transformer induction transducer, respectively. Three to five samples were tested for each material, temperature and type of bar (smooth or notched).

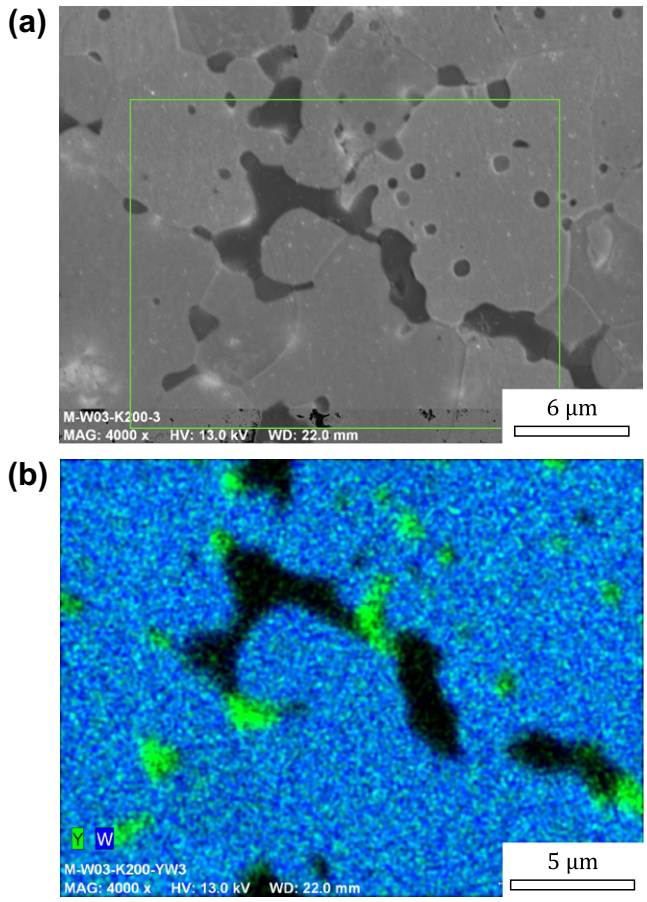

Fig. 3. Scanning electron micrograph of a polished section of the W–4Ti–0.5Y2O3 alloy showing the size and distribution of Y-oxide inclusions. (a) Secondary electrons image. (b) Mapping of W (blue) and Y (green) in the selected area of (a). The dark region corresponds to Ti. (For interpretation of the references to colour in this figure legend, the reader is referred to the web version of this article.)

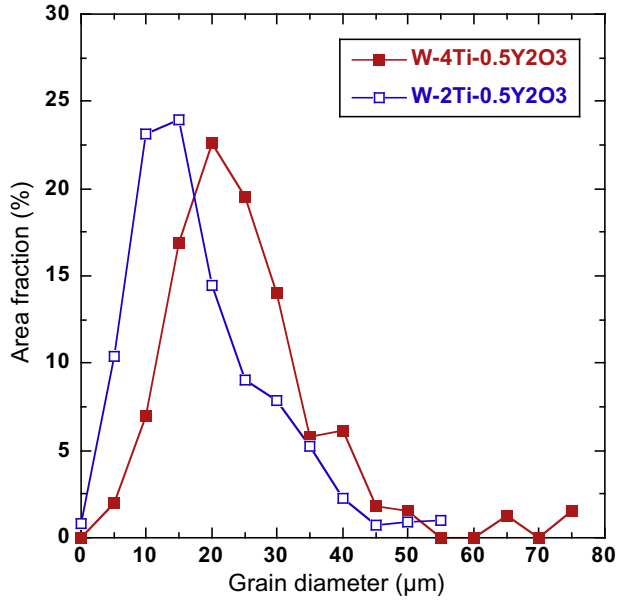

Fig. 4. Size distribution of the W grains.

Table 1
Vickers hardness.

Alloy	H_V (GPa) (9.8 N)	H_V (GPa) (98 N)
W ([15])		2.85 ± 0.10
W–4Ti ([12])	–	4.47 ± 0.03
W–4Ti–0.5Y_2O_3	3.55 ± 0.02	3.82 ± 0.01
W–2Ti–0.5Y_2O_3	3.14 ± 0.07	3.12 ± 0.04

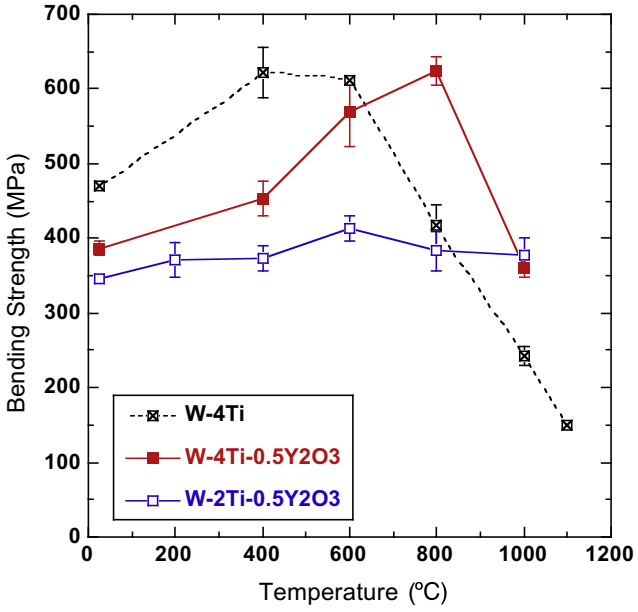

Fig. 5. Bending strength of the W–4Ti, W–2Ti–0.5Y_2O_3 and W–4Ti–0.5Y_2O_3 alloys tested in three-point bending as a function of temperature. The error bars correspond to the standard deviation of the experimental data.

The fracture surfaces of tested samples were analyzed in a scanning electron microscope. The analysis of the fracture surfaces was, however, hindered in the samples tested at 600 °C and above by the presence of an oxide layer. Thus, the broken specimens were cut through the middle and the cross-sections were mounted in epoxy resin and polished on SiC paper to 1000-grit finish and then on a diamond slurry, up to 1 μm. The polishing process finished on silica and specimens were cleaned in water and by ultrasound in acetone. The surfaces were etched with different reagents to determinate the microstructure and grain size (Murakami/Kroll and hydrogen peroxide/FH, respectively). They were studied in optical and scanning electron microscopes, the latter equipped with systems for energy dispersive X-ray microanalysis and electron backscattered diffraction, to analyze the microstructure and determine the dominant deformation and fracture micromechanisms as a function of the temperature. Samples were coated with Au by sputtering to improve the resolution in the scanning electron microscope.

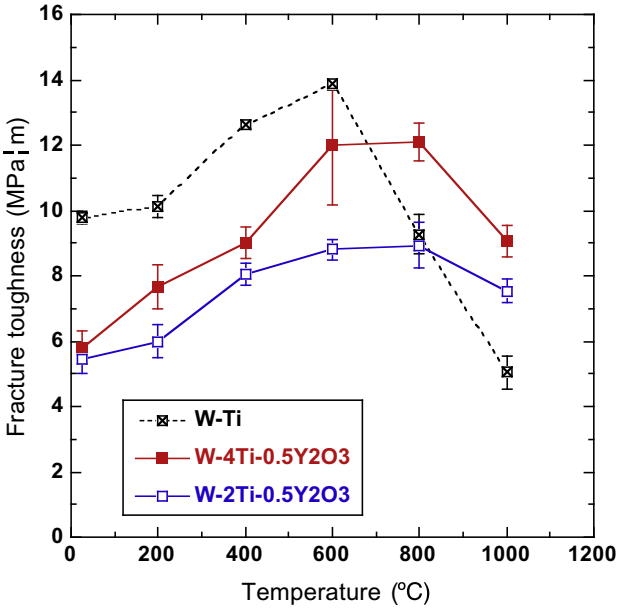

Fig. 6. Nominal fracture toughness of W–4Ti, W–2Ti–0.5Y_2O_3 and W–4Ti–0.5Y_2O_3 alloys tested as a function of temperature. The error bars correspond to the standard deviation of the experimental data.

3. Microstructure

The microstructures of the W–2Ti–0.5Y_2O_3 and W–4Ti–0.5Y_2O_3 materials are shown in Fig. 1. They are characterized by W particles (light grey) surrounded by a Ti(W) solid solution (dark grey) and sparsely distributed Ti pools (black). The Ti(W) solid solution is found surrounding the W particles in the W–4Ti–0.5Y_2O_3 alloy, Fig. 1b, whereas it is predominantly located around the larger Ti pools in the W–2Ti–0.5Y_2O_3 alloy, Fig. 1a. Energy-dispersive X-ray microanalyses revealed that the W content in Ti(W) solid solution was higher in W–4Ti–0.5Y_2O_3 than in W–2Ti–0.5Y_2O_3 and also than in the reference W–4Ti alloy processed following the same route and under the same conditions [4]. Moreover, the Ti pools in W–4Ti–0.5Y_2O_3 presented smaller size than in the reference

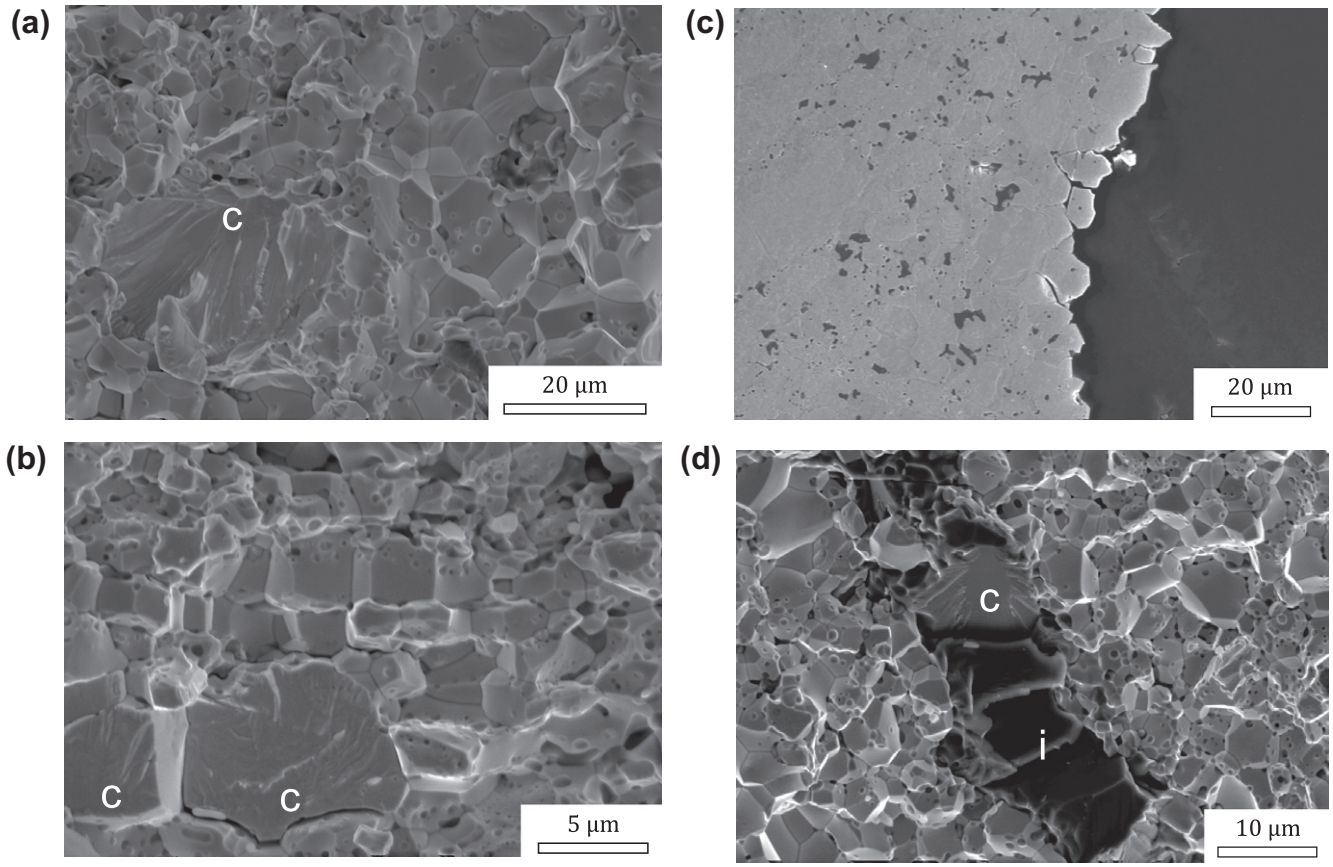

Fig. 7. (a) Fracture surface of W–4Ti–0.5Y_2O_3 alloy tested at ambient temperature showing intergranular cracking and cleavage (marked with c) of large W grains. (b) *Idem* for W–2Ti–0.5Y_2O_3. (c) Cross-section of the W–4Ti–0.5Y_2O_3 alloy showing the polygonal crack profile due to intergranular cracking. (d) Fracture of an elongated Ti pool in the W–2Ti–0.5Y_2O_3 alloy showing both intergranular cracking (marked with i) and cleavage (marked with c).

W–4Ti material [4], with a similar heterogeneous distribution. In the case of W–2Ti–0.5Y_2O_3, the Ti pools were elongated and appeared to be outlining preferentially orientated W grains (Fig. 1). Fig. 2 shows secondary electron images and EBSD patterns of W–4Ti–0.5Y_2O_3. The indexation of the EBSD patterns from the Ti(W) regions and Ti pools revealed that their crystal structure corresponded to hcp and bcc, respectively.

Inclusions of complex Y-oxides with different composition and a typical size of several microns were observed along the boundaries of the W grains and Ti pools (Fig. 3). Energy-dispersive X-ray analyses revealed different compositions of the complex Y-oxides: Ti–O–Y-oxides were found inside the Ti pools, whereas the oxides surrounding W grains were W-enriched. The morphology and distribution of these oxides appeared to be similar in both materials and point to their formation during sintering by an eutectic reaction. According to the phase diagram of the Ti–O system, this type of reaction can take place at ~1670 °C and ~1720 °C for O contents in liquid Ti of ~64 and ~57 at.%, respectively [25].

The size distribution of the W grains was measured in both alloys on etched, polished cross-section. The presence of the Ti(W) solid solution surrounding the W particles made it difficult to establish a good detection threshold of the particle boundaries, particularly for small grains. The area fraction as a function of the average grain diameter is plotted in Fig. 4 for both alloys. It shows wide distributions in both alloys with average grain sizes of 10–15 μm in W–2Ti–0.5Y_2O_3 and of 15–25 μm in W–4Ti–0.5Y_2O_3. These results indicate that higher Ti contents can activate grain growth when Y_2O_3 is present.

The density of the alloys was 16.545 ± 0.006 g/cm^3 and 16.76 ± 0.01 g/cm^3 for the W–2Ti–0.5Y_2O_3 and the W–4Ti–0.5Y_2O_3, respectively. They were slightly lower than those reported [4] for fully-dense materials, leading to porosities of 1.5% and 0.8% for W–2Ti–0.5Y_2O_3 and W–4Ti–0.5Y_2O_3, respectively. These results are in agreement with the observed residual microporosity.

4. Mechanical properties and failure micromechanisms

The values of the Vickers hardness for both alloys are shown in Table 1, which also includes the data in [20] and [17] for W and fully-dense W–4Ti, respectively, processed following the same route. The hardness values for pure W are similar to those reported in [21] for sintered W with densities in the range 87–92%. They are, obviously, much lower than those measured in fully-dense wrought W (which can reach 4.5 GPa [22]) whose yield strength has been increased by plastic deformation (extrusion, swaging, etc.). The addition of Ti substantially increased the hardness of W and this behavior is in agreement with nanohardness tests reported in [23], which showed that the nanohardness of the Ti(W) solid solution regions was significantly higher than that of pure W grains. The W–4Ti–0.5Y_2O_3 alloy hardness was slightly lower than that of W–4Ti and this difference could be attributed to the porosity of the former.

The smooth bars tested under three-point bending presented linear load–displacement curves until fracture in the whole temperature range studied (25–1000 °C). Thus, the bending strength was obtained from the Strength of Materials theory for an elastic beam of square cross-section. The average bending strength is plotted in Fig. 5 as a function of the temperature for both alloys, together with the results corresponding to the W–4Ti alloy reported in [17]. The toughness of the alloys as a function of temperature was assessed from three-point bending on notched bars. The load–displacement curves were also linear until fracture in the whole temperature range and the fracture toughness was computed from the maximum load and the initial notch length in each test using the appropriate expression for the stress intensity factor [24]. They are plotted as a function of temperature in Fig. 6, together with the results corresponding to the W–4Ti alloy [17]. They were in good agreement with those reported in the literature for W alloys manufactured by powder metallurgy [14].

The dominant failure mechanisms at ambient temperature were similar in both materials: intergranular cracking as well as fracture by cleavage of large W grains (Fig. 7a and b). The fracture surfaces also showed the presence of small intergranular pores. These brittle fracture mechanisms were responsible for the low toughness of the materials and led to a polygonal crack profile, as shown in Fig. 7c. The Ti pools were also fractured in a brittle manner with evidence of both intergranular cracking and cleavage (Fig. 7d). The strength and toughness of both alloys was significantly lower than that of the W–4Ti alloy in [17], which also presented equivalent failure micromechanisms. The differences can

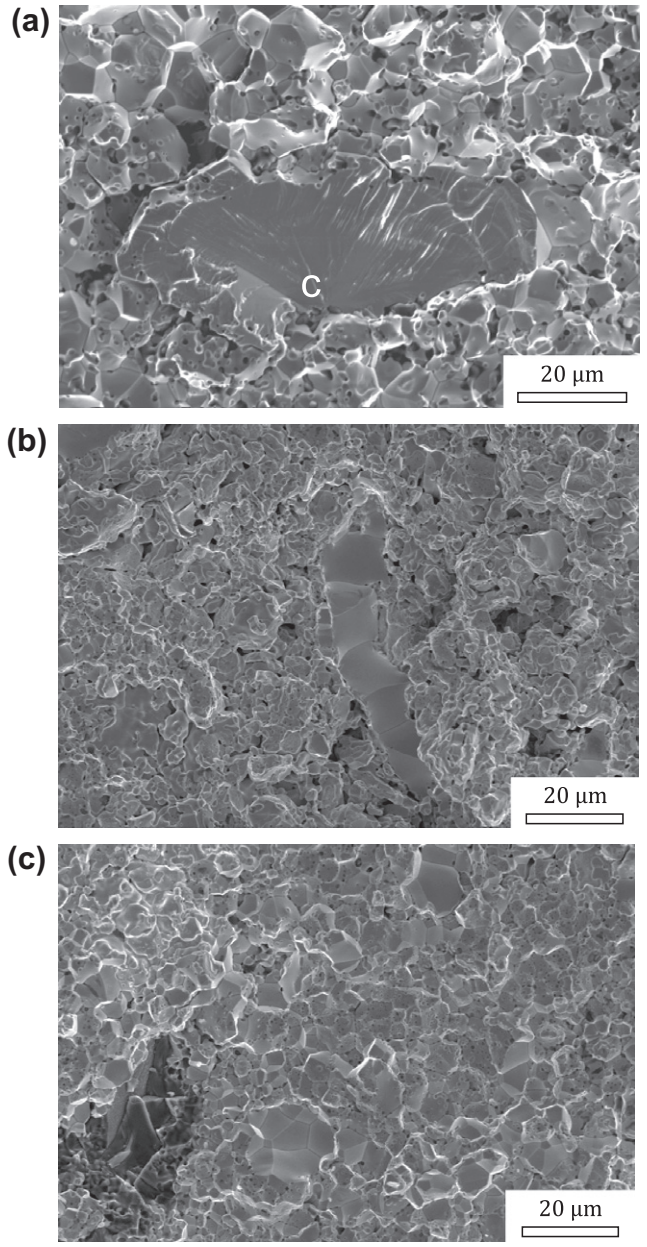

Fig. 8. (a) Fracture surface of W–4Ti–0.5Y_2O_3 alloy tested at 400 °C showing intergranular cracking and cleavage (marked with c) of a large W grain. (b) Fracture surface of W–2Ti–0.5Y_2O_3 alloy tested at 400 °C showing intergranular cracking in small and large W grains. (c) *Idem* at 600 °C.

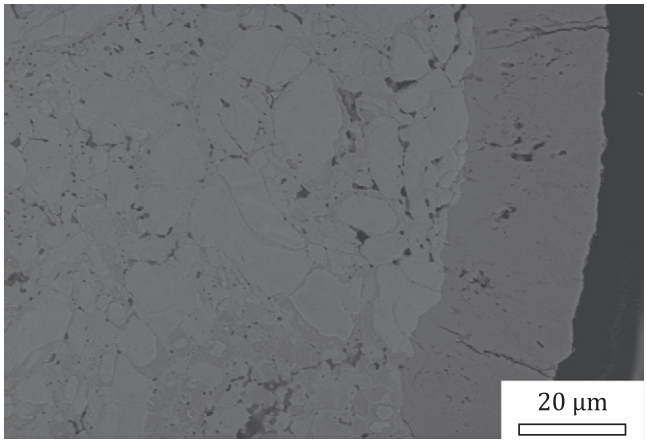

Fig. 9. Cross-section of a W–2Ti–0.5Y_2O_3 sample tested at 1000 °C showing the thick oxide layer on top of the fracture surface.

be attributed to the intergranular porosity in the W–4Ti–0.5Y_2O_3 W–2Ti–0.5Y_2O_3 samples, which promoted debonding between W grains. In addition, the average grain size of W–4Ti alloys was around 6 μm, much lower than that of the alloys in this paper. Finally, increasing the Ti content in the alloy did not significantly improve either the bending strength or the fracture toughness at ambient temperature, very probably because the alloy with higher Ti content also has the largest W grains which promoted early fracture by cleavage.

The toughness of W–Ti alloys improved with temperature (Fig. 6) and this effect increased with the Ti content. As a result of this, the bending strength also improved with temperature although the macroscopic behavior remained brittle. The analysis of the fracture surfaces at 400 °C and 600 °C showed that intergranular cracking was also the dominant failure mechanism, as at ambient temperature (Fig. 8a). Fracture of large W grains by cleavage was also found at these temperatures (Fig. 8a) but it was unusual. Mostly, the large W grains failed by intergranular cracking rather than by cleavage at 400 °C and 600 °C (Fig. 8b). Ti pools showed failure by intergranular cracking and cleavage up to 600 °C but they did not control the mechanical behavior. Thus, the improvement in toughness and (to a lesser extent) in strength in both alloys with temperature could be attributed to a change in the fracture initiation mechanisms in the large W grains from cleavage to intergranular cracking as the DBTT of W was approached.

This behavior is similar to that reported previously for W–Ti alloy [17] but oxidation rapidly degraded the mechanical behavior of this material above 600 °C. It was reported, however, that Y_2O_3 particles significantly improved the oxidation resistance of W alloys [15,19] and W–Y_2O_3 alloys were able to enhance the high temperature strength retention of W. The same phenomenon is observed in the case of W–Ti alloys, and the W–4Ti–0.5Y_2O_3 alloy overcame the mechanical performance of the W–4Ti counterpart at 800 °C even though they presented inferior strength and toughness at ambient temperature. The W–2Ti–0.5Y_2O_3, whose properties did not improve very much with temperature, presented excellent strength retention at high temperature, and its behavior at 800 °C and above was better than that of the W–4Ti alloy.

Oxidation of the fracture surfaces hindered the analysis of the fracture mechanisms at 800 °C and 1000 °C (Fig. 9) but the macroscopic behavior of the materials seems to indicate that there were no significant changes in the fracture micromechanisms in this temperature range. Fracture was brittle and the degradation in mechanical properties was controlled by the nucleation of defects by oxidation.

5. Conclusions

Two Y_2O_3-doped W–Ti alloys were manufactured by hot isostatic pressing using standard powder metallurgy techniques. Their mechanical properties (strength and toughness) were measured by means of three-point bending tests on smooth and notched bars from 25 °C up to 1000 °C in air. The microstructure of the alloys was characterized by W grains surrounded by a Ti(W) solid solution and sparsely distributed Ti pools. The size distribution of the W grains was wide and the materials presented some residual porosity.

The mechanical performance at ambient temperature was very brittle, in consonance with the failure mechanisms found in the fracture surfaces. Failure was initiated by cleavage fracture of large W grains and propagated by intergranular cracking. Both strength and toughness increased rapidly with temperature up to 600 °C while the number of large W grains broken by cleavage diminished. Failure at 400–600 °C was nucleated and propagated by intergranular cracking. Ti pools showed failure by intergranular cracking and cleavage in the whole temperature range and the mechanical properties improved with the Ti content. Thus, the improvement in toughness and (to a lesser extent) in strength in both alloys with temperature could be attributed to a change in the fracture initiation mechanisms in the large W grains from cleavage to intergranular cracking as the DBTT of W was approached. The mechanical properties were rapidly degraded above 600 °C due to oxidation. Nevertheless, it was confirmed that the presence of Y_2O_3 was very important to hindering oxidation and enhancing the strength retention at high temperature.

Acknowledgements

This investigation was supported by the EURATOM/CIEMAT association through Contract WP08-09-MAT-WWALLOY, by the Comunidad de Madrid (Programs ESTRUMAT-CM S2009/MAT-1585 and S2009/ENE-1679) and by Spanish Ministry of Science and Innovation (CSD00C-06-14102, MAT2009-13979-C03-02, MAT2007-29278-E).

References

[1] K. Krieger, H. Maier, R. Neu, J. Nucl. Mater. 266–269 (1999) 207.
[2] R. Dux, A. Herrmann, A. Kallenbach, R. Neu, J. Neuhauser, H. Maier, R. Pugno, T. Pütterich, V. Rohde, J. Nucl. Mater. 337–339 (2005) 852.
[3] R. Neu, A. Hopf, T. Kallenbach, T. Pütterich, R. Dux, H. Greuner, O. Gruber, A. Herrmann, K. Krieger, H. Maier, V. Rohde, J. Nucl. Mater. 367–370 (2007) 1497.
[4] P. Norajitra, L.V. Boccaccini, E. Diegele, V. Filatov, A. Gervash, R. Giniyatulin, S. Gordeev, V. Heinzel, G. Janeschitz, J. Konys, W. Kraus, R. Kruessmann, S. Malang, I. Mazul, A. Moeslang, C. Petersen, G. Reimann, M. Rieth, G. Rizzi, M. Rumyantsev, R. Ruprecht, V. Slobodtchouk, J. Nucl. Mater. 329–333 (2004) 1594.
[5] S.J. Zinkle, N.M. Ghoniem, J. Nucl. Mater. 51–52 (2000) 55.
[6] M. Rieth, B. Dafferner, J. Nucl. Mater. 342 (2005) 20.
[7] M.J. Makin, E. Gillies, J. Inst. Metals 86 (1957) 108.
[8] R.C. Koo, Trans. Metall. Soc. AIME 227 (1963) 280.
[9] P.L. Raffo, J. Less-Common Metals 17 (1969) 133.
[10] T. P. Herbell, J. W. Weeton, M. Quatinetz. NASA TN D-3610, 1966.
[11] J.M. Steichen, J. Nucl. Mater. 60 (1976) 13.
[12] M. Mabuchi, K. Okamoto, N. Saito, M. Nakanishi, Y. Yamada, T. Asahina, T. Igarashi, Mater. Sci. Eng. A 214 (1996) 174.
[13] M. Mabuchi, K. Okamoto, N. Saito, T. Asahina, T. Igarashi, Mater. Sci. Eng. A 237 (1997) 241.
[14] M. Faleschini, H. Kreuzer, D. Kiener, R. Pippan, J. Nucl. Mater. 367–370 (2007) 800.
[15] Y. Itoh, Y. Ishiwata, JSME Int. J. Series A 39 (1996) 429.
[16] Y. Kim, M.H. Hong, S.H. Lee, E.P. Kim, S. Lee, J.W. Noh, Metall. Mater. Int. 12 (2006) 245.
[17] M.V. Aguirre, A. Martin, J.Y. Pastor, J. LLorca, M.A. Monge, R. Pareja, Metall. Mater. Trans. 40A (2009) 2283.
[18] H. Bolt, V. Barabash, W. Krauss, J. Linke, R. Neu, S. Suzuki, N. Yoshida, J. Nucl. Mater. 329–333 (2004) 66.
[19] P. Pérez, G. Salmi, A. Muñoz, M.A. Monge, Scripta Mater. 60 (2009) 1008.

[20] M.A. Monge, M.A. Auger, T. Leguey, Y. Ortega, L. Bolzoni, E. Gordo, R. Pareja, J. Nucl. Mater. 386–388 (2009) 613.
[21] Y. Kim, M.H. Hong, et al., Metall. Mater. Int. 12 (2006) 245.
[22] S.A. Maloy, M.R. James, W.F. Sommer, G.J. Willcutt, M. Lopez, T.J. Romero, Mater. Trans. JIM 43 (2002) 633.
[23] M. A. Monge, T. Leguey, M. A. Auger, B. Savoini, Y. Ortega, R. Pareja, A. Muñoz, G. Salmi, L. Bolzoni, E. Gordo, Production of small laboratory scale batches of improved W alloys for characterization. Report TW6-TTMA002-D03, Carlos III University of Madrid, 2009.
[24] G. Guinea, J.Y. Pastor, J. Planas, M. Elices, Int. J. Fract. 89 (1998) 103.
[25] J.L. Murray (Ed.), Phase Diagrams of Binary Titanium Alloys, ASM International, Metal Park, Ohio, 1987. 211.